PCCP

Switchable electronic and enhanced magnetic properties of CrI3 edges

Journal:	*Physical Chemistry Chemical Physics*
Manuscript ID	CP-ART-11-2020-006155.R1
Article Type:	Paper
Date Submitted by the Author:	08-Mar-2021
Complete List of Authors:	Yang, Guohui; Shanxi Normal University, School of Physics and Information Engineering Wang, Rui; Shanxi Normal University Ge, Mei; Shanxi Normal University, School of Physics and Information Engineering Guo, Miaomiao; Shanxi Normal University, School of Physics and Information Engineering Wang, Jicui; Shanxi Normal University, School of Physics and Information Engineering Ma, Rongrong; Shanxi Normal University Zhang, Junfeng; Shanxi Normal University, School of Physics and Information Engineering West, Damien; Rensselaer Polytechnic Institute Zhang, Shengbai; Rensselaer Polytechnic Institute,

Switchable Electronic and Enhanced Magnetic Properties of CrI_3 Edges

Guohui Yang[a,b], Rui Wang[a,b], Mei Ge[a,b], Miaomiao Guo[a,b], Jicui Wang[a,b], Rongrong Ma[a,b], Junfeng Zhang[a,b]*, Damien West[c] and Shengbai Zhang[c*]

[a] School of Physics and Information Engineering, Shanxi Normal University, Linfen, 041004, China

[b] Key Laboratory of Spectral Measurement and Analysis of Shanxi Province, Shanxi Normal University, Linfen 041004, China

[c] Department of Physics, Applied Physics and Astronomy, Rensselaer Polytechnic Institute, Troy, NY 12180, USA

Corresponding Author

*E-mail address: zhangjf@sxnu.edu.cn (Junfeng Zhang), zhangs9@rpi.edu (Shengbai Zhang)

ABSTRACT

Owing to its novel electronic and magnetic properties, two-dimensional CrI_3 has great potential in application of spintronic devices. As an inevitable line defect, the properties of the edges of CrI_3, however, remain elusive. Here, by using first-principles calculations with spin-orbit coupling, we investigate the thermodynamic stabilities, electronic, and magnetic properties of thirteen CrI_3 edges with different structures. We show that zigzag edges are more stable than armchair edges, and a CrI_3 nanoribbon can be either metallic or insulating, depending on its chemical growth conditions. The edge stability and associated electronic properties can be understood in terms of the octahedron ligand field and electron counting model. In most cases, both the magnetic moment and Curie temperature can be enhanced by edges, which is in startle contrast to surfaces of three-dimensional ferromagnetic materials where a magnetic dead layer is often observed.

1. Introduction

Two-dimensional (2D) materials such as graphene[1] and MoS_2,[2] have attracted considerable interest because of their novel physical and chemical properties. Recently, the successful exfoliating of 2D intrinsic magnetic materials (CrI_3[3] and $CrGeTe_3$[4]) opened up a new avenue towards great applications in spintronics. In both material synthesis and device applications of the 2D materials, formation of edges is inevitable. It is therefore necessary to understand the effects of the edges on the electronic and magnetic properties of the 2D materials,[5] which will be valuable for novel device design.[6]

It is well-known that many properties of a 2D material can be determined by its edge. For example, an MoS_2 nanoribbon (NR) with armchair (AC) edges is a semiconductor,[5] but with zigzag (ZZ) edges it would be a metal.[7] Alternatively, by adsorption oxygen atoms at a 3× periodicity on the MoS_2 ZZ edges, the metallic NR can be tuned into a semiconductor with a band gap (Eg) of 1.23 eV.[8] Similarly, graphene NR can be either metallic or semiconducting, determined by edge type[9] and saturation.[10] As a matter of fact, the gap of a semiconducting NR can be tuned continuously by the NR width, in the range of 0.05-2.86 eV.[9] The magnetic properties of 2D materials can also be altered by the edge effect. For example, Xu et al.[11] demonstrated that, a magnetic moment of 1.02 μ_B can be achieved in graphene, by adsorbing hydrogen atoms on the ZZ edge. In 2H MoS_2 NR with a distorted 1T edge, a Mo-Klein edge, or a Mo-ZZ edge, the edge Mo atom presents a magnetic moment of 0.50, 1.01, and 0.90 μ_B, respectively.[12] Furthermore, it is possible to manipulate the catalytical[13] and optical[14] properties of 2D materials through an edge modification. Based on the principle of edge engineering, various prototypical nano devices have been suggested, such as negative differential resistance device[15] and transistors.[16]

2D magnetic materials have attracted attention also, especially after the successful exfoliation of 2D ferromagnetic (FM) CrI_3 in 2017.[3] It is worth to note that in a 2D nonmagnetic material, magnetic properties can be induced by manipulating the edge.[17, 18] For 2D FM materials, the edge effects can also be critical. Li et al. found that the 2H VS_2 NR with the ZZ edges is metallic but with the AC edges it becomes FM half-metallic, which is independent of the NR width.[19] In VSe_2 NR, a spin filtering effect has been observed along both the AC and ZZ directions.[20] For monolayer CrI_3, various properties including electronic,[21] magnetic,[22-24] thermoelectic,[25] and optical[26] properties have been extensively studied. Our recent work[27] also demonstrated a point defect-induced FM to antiferromagnetic (AFM) transition in CrI_3. As a line defect, edge can be expected to exhibit a greater influence on monolayer CrI_3 NR. Indeed, Wang et al.[28] found that, compared to its 2D counterpart, the Curie temperature (T_C) of CrI_3 NR is enhanced and becomes width-dependent, especially for those with the ZZ edges. Jiang et al.[29] have investigated theoretically such an edge effect as a function of the ribbon width (W). However, the edge structures of CrI_3 nanoribbon are more complex when compared with other 2D materials such as graphene or transition-metal dichalcogenides (TMDs), because of its six Cr ligands. Therefore, many issues about the edge effects on CrI_3 NRs are still unclear from our limited knowledge. For example, how do the edge atomic structure and stability change with different growth conditions and chemical stoichiometry? How do they influence the electronic and magnetic properties of the CrI_3 NR? Is the CrI_3 NRs metallic or semiconducting? And how changes of the edge magnetic moment and T_C?

In this paper, we clarify these questions by a comprehensive first-principles calculations on CrI_3 NRs. First, we assess the W effects on the edge structure. Second, we construct thirteen such structures and determine their thermodynamic stability based on the theory of phase diagram.

Finally, we explore the edge effects on the electronic and magnetic properties such as T_C of CrI_3 NRs.

2. Method

All calculations were based on the spin-polarized density functional theory (DFT) using the projector-augmented wave (PAW) potentials,[30, 31] as implemented in the Vienna Ab-initio Simulation Package (VASP).[32-34] The Perdew−Burke−Ernzerhof (PBE)[35] functional was used to describe the exchange-correlation interactions, and the plane-wave basis was expanded up to a cutoff energy of 400 eV. The vacuum region between neighboring edges was set to be at least 30 Å in the slab geometry. All structures were fully relaxed until the force on each atom was less than 0.01 eV/Å and the total energy was converged to 10^{-6} eV. The 2D Brillouin zone was sampled by 4×1×1 and 7×1×1 k-point grids for the AC and ZZ edges, respectively. Spin polarized calculations were carried out with the consideration of the effects of SOC for all the calculations. The DFT+U method of Dudarev[36] was used for interactions between Cr 3*d* orbitals in which we have used the on-site Coulomb parameter U = 2.7 eV and the exchange parameter J = 0.7 eV.[27, 37, 38]

3. Result and Discussion

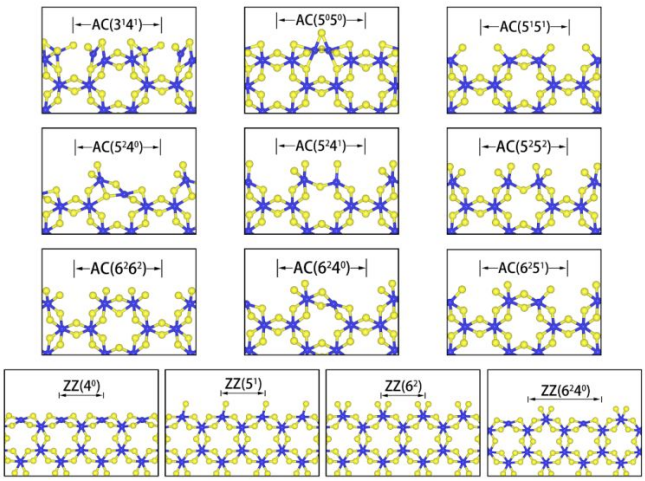

Figure 1. Thirteen edge structures for CrI_3 NR, fully optimized with SOC. Blue and yellow balls are Cr and I atoms, respectively. Period along the edge has been indicated by the arrow.

Chemical composition at edge can be different from bulk. Here, the edges are denoted by ($n1^{m1}n2^{m2}$), where n1 is the number of I atoms attached to Cr atom 1 at the edge and n2 is the number of I atoms attached to the next Cr (Cr atom 2) at the edge. Superscript m denotes the number of "dangling" I atoms which only bond to a particular Cr atom, 1 or 2, but not both. The CrI_3 NRs is obtained by cutting a CrI_3 monolayer. Depending on the cutting direction, the edges can be classified as predominately AC or ZZ type. At the NR edge, the chemical condition change makes ligancy of Cr atom different from that in bulk CrI_3. Here, we use the scheme ($n1^{m1}n2^{m2}$…) to describe the atomic structure of the edges. Details can be found in the caption of Figure 1 where thirteen CrI_3 NRs with different edges are depicted.

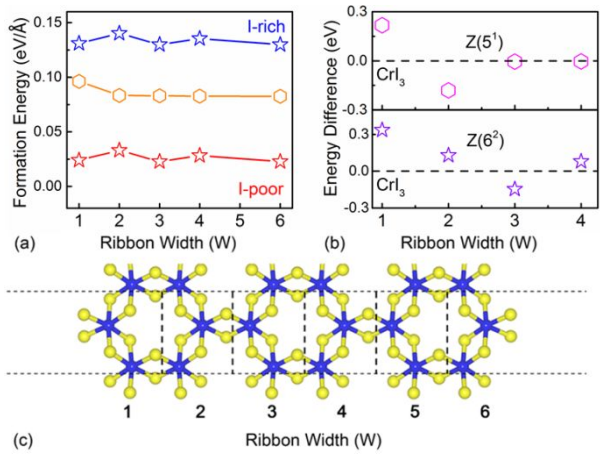

Figure 2. (a) Formation energy (E_{form}) and (b) energy difference between W+1 and W for ZZ(5^1) (open hexagons) and ZZ(6^2) (open stars) as a function of W. (c) A top view of ZZ(6^2) with W indicated.

To study individual edges, it is required to minimize interactions between the two edges of a NR. Here, taking ZZ(5^1) and ZZ(6^2) as examples, we have plotted E_{form} as a function of W in Figure 2a. Note that ZZ(5^1) is stoichiometric and as such E_{form} is independent of μ_I. In contrast, ZZ(6^2) is not stoichiometric so there are two E_{form}'s, corresponding to I-rich and I-poor. We see that, with an increasing W, E_{form} quickly converges to 0.08 eV/Å for ZZ(5^1). The same is true for ZZ(6^2), in which E_{form} converges to 0.02 eV/Å under I poor, and 0.13 eV/Å under I rich. Figure 2a also indicated that, E_{form} of ZZ(6^2) with odd W (with asymmetric edges) is slightly lower (< 0.018 eV/Å) than that with even W (symmetric edges). To visualize the convergence of the calculation, Figure 2b plot the energy differences between W and W+1 NRs for ZZ(5^1) and ZZ(6^2), respectively. For W = 4, the energy differences in both ZZ(5^1) and ZZ(6^2) are reasonably close to that calculated for perfect CrI_3 by 0.00 and 0.04 eV, respectively. In agreement with previous study of graphene NR,[39] edge-edge interaction quickly diminishes for W $\geqslant$ 4 (~ 24 Å). Hence, W = 4 has been selected here for all structural calculations of the CrI_3 NRs.

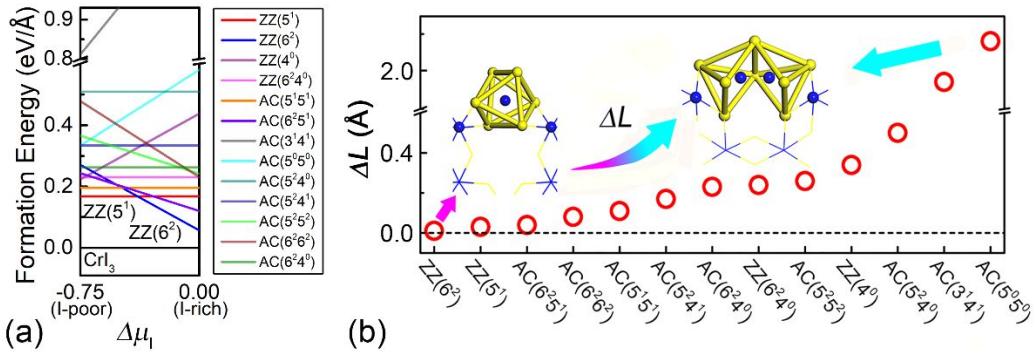

Figure 3. E_{form} (a) and (b) the Cr-Cr bond length difference (ΔL) between those in bulk and at edge of thirteen CrI_3 NRs. The insets show the shapes of OLFat the edge of ZZ(6^2) and AC($5^0 5^0$) structures.

To elucidate the thermodynamic stability of thirteen edge geometry, we define the E_{form} of the edge [27, 40-43] as:

$$E_{\text{form}} = (E_{\text{tot}}^{\text{edge}} - E_{\text{tot}}^{\text{per}} \pm N\mu_{\text{I}})/2L, \tag{1}$$

where $E_{\text{tot}}^{\text{edge}}$ is the total energy of a NR, $E_{\text{tot}}^{\text{per}}$ is that of a perfect CrI_3 with the same number of Cr atoms as the NR, L is the NR length, and μ_{I} is the chemical potential of iodine. Note that a NR may not be stoichiometric as its bulk due to edge reconstruction, leading to an excess (–) or deficiency (+) of I atoms, termed here N. The varied μ_{I} is determined by the formation of CrI_3 from bulk Cr and I_2 gas systems, in other words, the chemical potential of Cr (I) atom μ_{Cr} (μ_I) in CrI_3 satisfies: $\mu(\text{CrI}_3) = \mu_{\text{Cr}} + 3\mu_{\text{I}}$, in which $\mu(\text{CrI}_3)$ is the total energy of CrI_3 monolayer per (CrI_3) atoms. Meanwhile, $\mu_{\text{Cr}} = \Delta\mu_{\text{Cr}} + \mu_{\text{Cr}}^{\text{bulk}}$ and $\mu_{\text{I}} = \Delta\mu_{\text{I}} + \mu(I_2)/2$, where $\mu_{\text{Cr}}^{\text{bulk}}$ is the total energy per Cr atom in its elemental bulk structure, and $\mu(I_2)$ is the total energy per I_2 molecule.[49] Therefore, we define Gibbs energy of formation (ΔG) as:

$$\Delta G = \Delta\mu_{\mathrm{Cr}} + 3\Delta\mu_{\mathrm{I}}. \quad (2)$$

Under this definition, the chemical potential of I can vary from I rich ($\Delta\mu_{\mathrm{I}} = 0$) to I poor (i.e., Cr rich with $\Delta\mu_{\mathrm{Cr}} = 0$, which implies that $\Delta\mu_{\mathrm{I}} = \Delta G/3 = -0.75$ eV). Note that the SOC effect have been included for the more reasonable E_{form}, as suggested in our previous work.[27]

For the relaxed structures in Figure 1, Figure 3a shows the corresponding E_{form}. Inside a CrI_3, each Cr atom is surrounded by 6 first nearest-neighbor I atoms arranged in a corner sharing octahedra, which results in an octahedral ligand field (OLF). Correspondingly, the fivefold degenerate atomic *d* levels of Cr split into a higher-energy e_{g} doublet and a lower-energy $t_{2\mathrm{g}}$ triplet. Meanwhile, according to the electron counting model (ECM),[8] in monolayer CrI_3, each Cr atom donates 3 electrons to its 6 nearest-neighbor I atoms (1/2 electrons per I atom), and each I accept 1 electron from its 2 nearest-neighbor Cr atoms. At the edge, however, both OLF and the network of neighbors (i.e., 6 I for Cr and 2 Cr for I) are broken, making the edge energy higher.

We discuss the geometry structure and E_{form} of CrI_3 NR based on OLF and ECM at edges: (i) Good conservation of the OLF at edges compared with that inside the NR, such as AC($5^1 5^1$), AC($6^2 6^2$), AC($6^2 5^1$), ZZ(5^1), and ZZ(6^2). There is no clear dependence between the I-Cr-I bond angle at the edge region and E_{form}. Therefore, in Figure 3b, we use the maximum change of Cr-Cr bond length ($\Delta L = |L_{\mathrm{Cr\text{-}Cr}}(\mathrm{edge}) - L_{\mathrm{Cr\text{-}Cr}}(\mathrm{bulk})|$) to measure the conservation of the OLF. For ZZ(6^2), only 0.01 Å in ΔL can be found, which suggested little change in octahedron configuration (inset of Figure 3b). For ZZ(5^1) (Figure 1), Cr donates 3 electrons to its 5 nearest neighbor I atoms, 4 of I atoms accept 2 electrons and the dangling I atom accept 1 electron, ECM is satisfied. Therefore, ZZ(6^2) (0.02–0.13 eV/Å) and ZZ(5^1) (0.08 eV/Å) possess the lowest E_{form} at I-rich and I-poor chemical environment, respectively. Clearly, E_{form} of CrI_3 NR edge from this

calculation are much lower than that of graphene (> 1eV/Å)[44] or MoS_2 NR (> 0.81 eV).[12] (ii) The slightly disturbed of OLF, which induced self-passivated through edge reconstruction, such as AC($5^2 4^1$), AC($5^2 5^2$), AC($6^2 4^0$), ZZ(4^0) and ZZ($6^2 4^0$). As plotted in Figure 3, ΔL and E_{form} at the range of (0.17, 0.34 Å) and (0.11, 0.22 eV/Å), respectively. (iii) The broken of OLF in AC($3^1 4^1$), AC($5^0 5^0$) and AC($5^2 4^0$). All the three NRs have bare Cr edge, in which the edge Cr donates 2 electrons to the 4 neighbor I atoms and one unpaired electron for each edge Cr atom compared with that inside the NR. Both OLF and ECM are unsatisfied. The extra one unpaired electron of Cr atom makes the $L_{Cr\text{-}Cr}$(edge) shorter and breaks OLF, which can be found in the inset of Figure 3b. Overall, we can conclude that, consistent with MoS_2 NR,[12] ZZ edges of CrI_3 NR possess the lower E_{form} compared with AC edges.

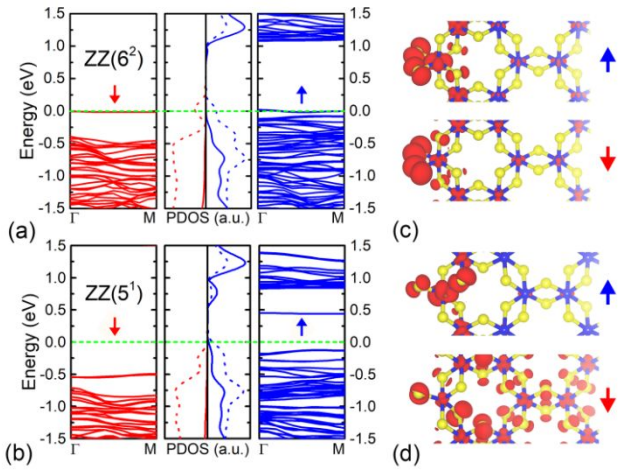

Figure 4. The electronic structures (a, b) and partial charge density (c, d) of CrI_3 NR ZZ(6^2) (a, c) and ZZ(5^1) (b, d), respectively. The partial charge densities indicate contribution from bands of ZZ(6^2) at the E_F (c) and valence-band maximum (VBM) of ZZ(5^1) (d), blue and red arrow labeled spin-up and spin-down state, and solid and dashed line in PDOS stands for the contributions from Cr-3*d* orbital and I-5*p* orbital, respectively. The isosurface is set to 2×10^{-3} e/Å^3 in (c) and (d).

In Figure 4, we analysis the electronic structures of CrI_3 NR with the most energetically favorable edges ZZ(6^2) and ZZ(5^1). As shown in Figure 1, for ZZ(6^2), each edge Cr atom bonds with 6 neighbor I atoms, 2 of which are dangling I atoms. Note that, in fully optimized ZZ(6^2), the bond length between the two dangling I atoms is 3.40 Å, which is larger than that (2.68Å) in I_2 molecule. Moreover, no obvious charge density overlaps between the two dangling I atoms from the charge density. Each edge Cr atom in ZZ(6^2) donates (6×1/2) electrons to 6 neighbor I atoms, and need one more electron to form the outside closed shell for the 2 dangling I atoms. Therefore, spin-up and spin-down states near the Fermi level in Figure 4a are mainly contributed from the two dangling I atoms as present in Figure 4c. Differently, previously research suggested that CrI_3 ZZNR (ZZ(6^2)) is a semiconductor (~0.71 eV),[28, 29] which is contradict with the ECM picture. However, as discussed above, ECM is good satisfied for ZZ(5^1). Thus, the edge states can be eliminated in ZZ(5^1) and semiconducting properties can be expected. The DFT calculation confirmed that, ZZ(5^1) is a semiconductor with a band gap of 0.6 eV (Figure 4b), and the VBM for both spin-up and spin-down states are delocalized (Figure 4d), especially for spin-down states. Our results reveal that, either metallic or semiconducting edge in CrI_3 NR is possible, depends on the chemical potential of I atoms.

Table 1. Nearest neighbor bond length of Cr−Cr (L_{Cr-Cr}, Å) and Cr−I (L_{Cr-I}, Å) at edges, T_C (K), magnetic moments for (averaged, edge) (M, μ_B/Cr), and magnetic phase (FM/AFM) of thirteen CrI_3 NRs with the comparison of those in bulk CrI_3.

Edge	L_{Cr-Cr} (Å)	L_{Cr-I} (Å)	T_C (K)	M (μ_B/Cr)	Phase
CrI_3	4.04	2.67	49	3.00	FM
AC($3^1 4^1$)	2.07	2.50	-	(0.10, 0.67)	AFM
AC($5^0 5^0$)	1.96	3.02	-	(0.00, 0.91)	AFM
AC($5^1 5^1$)	3.93	2.57	57	(3.05, 3.04)	FM
AC($5^2 4^0$)	3.54	2.58	50	(3.13, 3.31)	FM
AC($5^2 4^1$)	3.87	2.52	58	(3.03, 3.05)	FM
AC($5^2 5^2$)	4.30	2.59	82	(3.03, 2.97)	FM
AC($6^2 6^2$)	4.12	2.53	64	(2.89, 2.69)	FM
AC($6^2 4^0$)	3.81	2.62	53	(3.09, 3.20)	FM
AC($6^2 5^1$)	4.00	2.67	54	(3.02, 2.92)	FM
ZZ(4^0)	3.70	2.66	80	(3.10, 3.59)	FM
ZZ(5^1)	4.01	2.58	88	(3.10, 3.03)	FM
ZZ(6^2)	4.03	2.68	105	(3.04, 2.96)	FM
ZZ($6^2 4^0$)	3.80	2.90	50	(3.08, 3.22)	FM

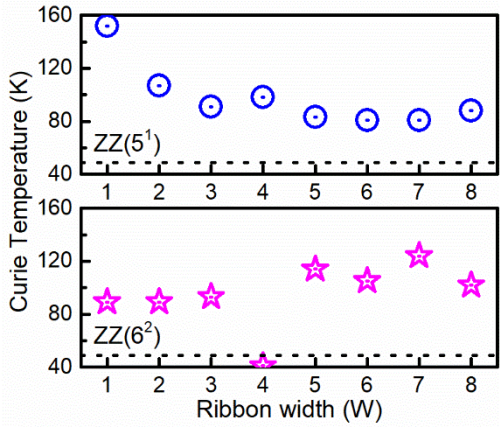

Figure 5. Variation of T_C for ZZ(5^1) (upper) and ZZ(6^2) (lower) CrI_3 NR as a function of the changes W. The dash line represents the T_C of perfect CrI_3.

Table 1 listed the magnetic properties of different CrI_3 NRs, such as T_C, magnetic moments (M) and the stable magnetic phase. Except AC(3^14^1) and AC(5^05^0), FM magnetic phase remained for other edges. $L_{Cr\text{-}Cr}$ pose 2.07 and 1.96 Å at the edge of AC(3^14^1) and AC(5^05^0), respectively. We thus propose the FM to AFM transition here is mainly result from local strain at edges, similar with the point defect induced transition in monolayer CrI_3[27]. Mostly, for the FM CrI_3 NRs, the M of Cr at the edge are resemble those interior Cr with deviation of 0.33–15.81%. It is found that about 1 μ_B can be induced in MoS_2 NR.[12] On the contrary, in ferromagnetic manganite nanoparticles,[45] M of the edge atoms can be eliminated and form a magnetic "dead layer".

As one parameter of magnetic properties, T_C of CrI_3 NR is vital for the practical application of information storage devices. Therefore, we explore the variation of T_C by adopting the simple Ising model with the consideration of nearest neighbor exchange interactions. The Hamiltonian here can be defined as:

$$H = \sum_{nn} J_1 \overrightarrow{S_1} \cdot \overrightarrow{S_2}, \tag{3}$$

in which S is the spin operator, J_1 is the nearest neighbor exchange parameters. Take a (2×2×1) supercell of perfect CrI_3 as an example, the eigenvalue of different magnetic phases is indicated as:

$$E_{FM} = 12J_1S^2, \tag{4}$$

$$E_{Néel} = -12J_1S^2, \tag{5}$$

E_{FM} and $E_{Néel}$ are the total energy of FM and Néel-AFM.[23] Then, with S = 3/2 for Cr atoms in perfect CrI_3, we can obtain: $J_1 = (E_{FM} - E_{Néel})/24S^2 = -2.751$ meV. In agreement with the

experimental measurement T_C of 45 K,[3] our Ising model[46] on perfect CrI_3 gives T_C=49 K. Note that, because of the nearest neighbor number of the edged Cr is different from those of interior Cr atoms for CrI_3 NR, the detailed expressions (eq.4-5) and then J_1 are different from that in perfect CrI_3. For ZZ(6^2), E_{FM} and $E_{Néel}$ is $32J_1$ and $-34J_1$, respectively. Therefore, the nearest neighbor exchange parameter for ZZ(6^2) is $J_1 = (E_{FM} - E_{Néel})/66S^2 = -5.694$ meV, which induce 105 K of T_C by the Ising model. Similarly, we can estimate T_C for all FM CrI_3 NRs, as listed in Table 1. All CrI_3 NRs considered in this work possess the higher T_C (50 – 105 K) than perfect CrI_3. Figure 5 plotted T_C with different W for the ZZ(5^1) and ZZ(6^2) CrI_3 NR. It can be found that, T_C of CrI_3 NR is basically higher than that of perfect CrI_3 when W $\geqslant$ 5, and none obvious linear behaviour between Tc and W. This is in startle contrast to surfaces of three-dimensional FM materials, where a magnetic dead layer is often observed.[47, 48] Noteworthy, T_C of CrI_3 ribbon should approach to that of perfect CrI_3 monolayer with the increase of W ($\sim \infty$). However, compare with that of perfect CrI_3, T_C at have been increased by 114% and 79% for the most energetically favorable ZZ(6^2) and ZZ(5^1) with W = 8, respectively. We found that, the energy difference between FM and AFM for ZZ(5^1) and ZZ(6^2) have similar behaviours with T_C. Therefore, a larger W is needed for the converged T_C.

4. Conclusions

In summary, the atomic structures, thermodynamic stabilities, electronic and magnetic properties of CrI_3 edges have been investigated by using the first-principle calculations. Our results demonstrated that ZZ type edges, such as ZZ(5^1) and ZZ(6^2), are more energetically favorable than AC types. Meanwhile, metallic or semiconducting edge can be obtained at different chemical conditions. The atomic and electronic structures of CrI_3 NR edges are comprehensible with the help of OLF and ECM. Our results also suggested that, most stable edges remain FM phase, with enhanced magnetic moments and T_C compared with that of perfect CrI_3. Our theoretical research provides theoretical support for the synthetic of CrI_3 edges and useful for developing nanoscale electronics and spintronics.

Associated Content

Author Information

Junfeng Zhang - School of Physics and Information Engineering, Shanxi Normal University, Linfen, 041004, China; Key Laboratory of Spectral Measurement and Analysis of Shanxi Province, Shanxi Normal University, Linfen 041004, China.

Email: zhangjf@sxnu.edu.cn

Shengbai Zhang - Department of Physics, Applied Physics and Astronomy, Rensselaer Polytechnic Institute, Troy, NY 12180, USA.

Email: zhangs9@rpi.edu

Authors

Guohui Yang - School of Physics and Information Engineering, Shanxi Normal University, Linfen, 041004, China; Key Laboratory of Spectral Measurement and Analysis of Shanxi Province, Shanxi Normal University, Linfen 041004, China

Wang Rui - School of Physics and Information Engineering, Shanxi Normal University, Linfen, 041004, China; Key Laboratory of Spectral Measurement and Analysis of Shanxi Province, Shanxi Normal University, Linfen 041004, China

Mei Ge - School of Physics and Information Engineering, Shanxi Normal University, Linfen, 041004, China; Key Laboratory of Spectral Measurement and Analysis of Shanxi Province, Shanxi Normal University, Linfen 041004, China

Miaomiao Guo - School of Physics and Information Engineering, Shanxi Normal University, Linfen, 041004, China; Key Laboratory of Spectral Measurement and Analysis of Shanxi Province, Shanxi Normal University, Linfen 041004, China

JiCui Wang - School of Physics and Information Engineering, Shanxi Normal University, Linfen, 041004, China; Key Laboratory of Spectral Measurement and Analysis of Shanxi Province, Shanxi Normal University, Linfen 041004, China

Rongrong Ma - School of Physics and Information Engineering, Shanxi Normal University, Linfen, 041004, China; Key Laboratory of Spectral Measurement and Analysis of Shanxi Province, Shanxi Normal University, Linfen 041004, China

Damien West - Department of Physics, Applied Physics and Astronomy, Rensselaer Polytechnic Institute, Troy, NY 12180, USA.

Author Contributions

The manuscript was written through contributions of all authors. All authors have given approval to the final version of the manuscript.

Notes

The authors declare no competing financial interest.

Acknowledgment

Work in China was supported by the National Natural Science Foundation of China (12074235) and Shanxi Scholarship Council of China (HGKY2019049). S.Z. was supported by the United States Department of Energy (US-DOE) under grant no. DESC0002623.

References

(1) Geim., A. K.; Novoselov., K. S. The Rise of Graphene. *Nat. Mater.* 2007, **6**, 183–191.

(2) Lebègue, S.; Eriksson, O. Electronic Structure of Two-Dimensional Crystals Fromab Initiotheory. *Phys. Rev. B* 2009, **79**, 115409.

(3) Huang, B.; Clark, G.; Navarro-Moratalla, E.; Klein, D. R.; Cheng, R.; Seyler, K. L.; Zhong, D.; Schmidgall, E.; McGuire, M. A.; Cobden, D. H.; Yao, W.; Xiao, D.; Jarillo-Herrero, P.; Xu, X. Layer-Dependent Ferromagnetism in a van der Waals Crystal Down to the Monolayer Limit. *Nature* 2017, **546**, 270-273.

(4) Gong, C.; Li, L.; Li, Z.; Ji, H.; Stern, A.; Xia, Y.; Cao, T.; Bao, W.; Wang, C.; Wang, Y.; Qiu, Z. Q.; Cava, R. J.; Louie, S. G.; Xia, J.; Zhang, X. Discovery of Intrinsic Ferromagnetism in Two-Dimensional van der Waals Crystals. *Nature* 2017, **546**, 265-269.

(5) Pan, H.; Zhang, Y. Edge-Dependent Structural, Electronic and Magnetic Properties of MoS_2 Nanoribbons. *J. Mater. Chem.* 2012, **22**, 7280-7290.

(6) Ren, H.; Li, Q.; Luo, Y.; Yang, J. Graphene Nanoribbon as a Negative Differential Resistance Device. *Appl. Phys. Lett.* 2009, **94**, 173110-173113.

(7) Davelou, D.; Kopidakis, G.; Kaxiras, E.; Remediakis, I. N. Nanoribbon Edges of Transition-Metal Dichalcogenides: Stability and Electronic Properties. *Phys. Rev. B* 2017, **96**, 165436.

(8) Lucking, M. C.; Bang, J.; Terrones, H.; Sun, Y.; Zhang, S. Multivalency-Induced Band Gap Opening at MoS_2 Edges. *Chem. Mater.* 2015, **27**, 3326-3331.

(9) Magda, G. Z.; Jin, X.; Hagymasi, I.; Vancso, P.; Osvath, Z.; Nemes-Incze, P.; Hwang, C.; Biro, L. P.; Tapaszto, L. Room-Temperature Magnetic Order on Zigzag Edges of Narrow Graphene Nanoribbons. *Nature* 2014, **514**, 608-611.

(10) Sun, Y. Y.; Ruan, W. Y.; Gao, X.; Bang, J.; Kim, Y.-H.; Lee, K.; West, D.; Liu, X.; Chan, T. L.; Chou, M. Y.; Zhang, S. B. Phase Diagram of Graphene Nanoribbons and Band-Gap Bifurcation of Dirac Fermions under Quantum Confinement. *Phys. Rev. B* 2012, **85**, 195464.

(11) Xu, B.; Yin, J.; Xia, Y. D.; Wan, X. G.; Jiang, K.; Liu, Z. G. Electronic and Magnetic Properties of Zigzag Graphene Nanoribbon with One Edge Saturated. *Appl. Phys. Lett.* 2010, **96**, 163102.

(12) Zhao, X.; Fu, D.; Ding, Z.; Zhang, Y. Y.; Wan, D.; Tan, S. J. R.; Chen, Z.; Leng, K.; Dan, J.; Fu, W.; Geng, D.; Song, P.; Du, Y.; Venkatesan, T.; Pantelides, S. T.; Pennycook, S. J.; Zhou, W.; Loh, K. P. Mo-Terminated Edge Reconstructions in Nanoporous Molybdenum Disulfide Film. *Nano Lett.* 2018, **18**, 482-490.

(13) Ni, B.; Wang, X. Face the Edges: Catalytic Active Sites of Nanomaterials. *Adv Sci (Weinh)* 2015, **2**, 1500085.

(14) Ostovari, F.; Moravvejfarshi, M. K. J. A. P. L. Dual Function Armchair Graphene Nanoribbon-Based Spin-Photodetector: Optical Spin-Valve and Light Helicity Detector. *Appl. Phys. Lett.* 2014, **105**, 072407.

(15) Ren, H.; Li, Q.; Luo, Y.; Yang, J. J. A. P. L. Graphene Nanoribbon as a Negative Differential Resistance Device. *Appl. Phys. Lett.* 2009, **94**, 173110-173113.

(16) Liu, H.; Gu, J.; Ye, P. D. MoS_2 Nanoribbon Transistors: Transition From Depletion Mode to Enhancement Mode by Channel-Width Trimming. *IEEE Electron Device Lett.* 2012, **33**, 1273-1275.

(17) Wang, J.; Jiang, W.; Zhou, C.; Shi, Z.; Wu, C. J. S.; Microstructures Magnetic Properties of a Nanoribbon: An Effective-Field Theory. *Superlattices Microstruct.* 2017, **102**, 359-372.

(18) Liu, W.; Zheng, J.; Zhao, P.; Cheng, S.; Guo, C. Magnetic Properties of Silicene Nanoribbons: A DFT Study. *AIP Adv.* 2017, **7**, 065004.

(19) Li, F.; Tu, K.; Chen, Z. Versatile Electronic Properties of VSe_2 Bulk, Few-Layers, Monolayer, Nanoribbons, and Nanotubes: A Computational Exploration. *J Phys. Chem. C* 2014, **118**, 21264-21274.

(20) Zhang, W.; Sun, W. Spintronic Transport Performances of VSe_2 Nanoribbons. *J. Nanoelectron. Optoelectron.* 2020, **15**, 269-275.

(21) Jiang, P.; Li, L.; Liao, Z.; Zhao, Y. X.; Zhong, Z. Spin Direction-Controlled Electronic Band Structure in Two-Dimensional Ferromagnetic CrI_3. *Nano Lett.* 2018, **18**, 3844-3849.

(22) Jiang, S.; Li, L.; Wang, Z.; Mak, K. F.; Shan, J. Controlling Magnetism in 2D CrI_3 by Electrostatic Doping. *Nat. Nanotechnol.* 2018, **13**, 549-553.

(23) Zheng, F.; Zhao, J.; Liu, Z.; Li, M.; Zhou, M.; Zhang, S.; Zhang, P. Tunable Spin States in the Two-Dimensional Magnet CrI_3. *Nanoscale* 2018, **10**, 14298-14303.

(24) Yang, B.; Zhang, X.; Yang, H.; Han, X.; Yan, Y. Nonmetallic Atoms Induced Magnetic Anisotropy in Monolayer Chromium Trihalides. *J Phys. Chem. C* 2018, **123**, 691-697.

(25) Gao, B.; Zhou, T.; Hong, A.; Liang, F.; Song, G.; Xu, Q.; Zhang, J.; Li, G.; Wang, Y.; Dang, C. J. A. P. E. Study on Thermoelectric Properties of CrI_3 Monolayer. *Appl. Phys Express* 2020, **13**, 045001.

(26) Huang, B.; Cenker, J.; Zhang, X.; Ray, E. L.; Song, T.; Taniguchi, T.; Watanabe, K.; McGuire, M. A.; Xiao, D.; Xu, X. Tuning Inelastic Light Scattering via Symmetry Control in the Two-Dimensional Magnet CrI_3. *Nat. Nanotechnol.* 2020, **15**, 212-216.

(27) Wang, R.; Su, Y.; Yang, G.; Zhang, J.; Zhang, S. Bipolar Doping by Intrinsic Defects and Magnetic Phase Instability in Monolayer CrI_3. *Chem. Mater.* 2020, **32**, 1545-1552.

(28) Wang, J.; Huang, J.; Wang, Y.; Yang, T.; Zhang, Z. Electronic and Magnetic Properties of CrI_3 Nanoribbons and Nanotubes. *Chin. Phys. B* 2019, **28**, 077301.

(29) Jiang, W.; Li, S.; Liu, H.; Lu, G.; Zheng, F.; Zhang, P. First-Principles Calculations of Magnetic Edge States in Zigzag CrI_3 Nanoribbons. *Phys. Lett. A* 2019, **383**, 754-758.

(30) Blöchl, P. E. Projector Augmented-Wave Method. *Phys. Rev. B* 1994, **50**, 17953-17979.

(31) G, K.; D, J. From Ultrasoft Pseudopotentials to the Projector Augmented-Wave Method. *Phys. Rev. B* 1999, **59**, 1758.

(32) Kresse, G.; Hafner, J. Ab Initio Molecular-Dynamics Simulation of the Liquid-Metal–Amorphous-Semiconductor Transition in Germanium. *Phys. Rev. B* 1994, **49**, 14251.

(33) Kresse, G.; Furthmüller, J. Efficient Iterative Schemes for Ab Initio Total-Energy Calculations Using a Plane-Wave Basis Set. *Phys. Rev. B* 1996, **54**, 11169.

(34) Kresse, G.; Furthmüller, J. Efficiency of Ab-Initio Total Energy Calculations for Metals and Semiconductors Using a Plane-Wave Basis Set. *Comput. Mater. Sci* 1996, **6**, 15-50.

(35) P, P. J.; K, B.; M, E. Generalized Gradient Approximation Made Simple. *Phys. Rev. Lett.* 1996, **77**, 3865.

(36) Dudarev, S.; Botton, G.; Savrasov, S.; Humphreys, C.; Sutton, A. Electron-Energy-Loss Spectra and the Structural Stability of Nickel Oxide: An LSDA+ U Study. *Phys. Rev. B* 1998, **57**, 1505.

(37) Ge, M.; Su, Y.; Wang, H.; Yang, G.; Zhang, J. Interface Depended Electronic and Magnetic Properties of Vertical CrI_3/WSe_2 Heterostructures. *RSC Adv.* 2019, **9**, 14766-14771.

(38) Bultmark, F.; Cricchio, F.; Grånäs, O.; Nordström, L. Multipole Decomposition of LDA+Uenergy and Its Application to Actinide Compounds. *Phys. Rev. B* 2009, **80**, 035121.

(39) Koskinen, P.; Malola, S.; Hakkinen, H. Self-Passivating Edge Reconstructions of Graphene. *Phys. Rev. Lett.* 2008, **101**, 115502.

(40) Haldar, S.; Vovusha, H.; Yadav, M. K.; Eriksson, O.; Sanyal, B. Systematic Study of Structural, Electronic, and Optical Properties of Atomic-Scale Defects in the Two-Dimensional Transition Metal Dichalcogenides MX_2 (M = Mo, W; X = S, Se, Te). *Phys. Rev. B* 2015, **92**, 235408.

(41) Han, N.; Liu, H.; Zhou, S.; Zhao, J. Possible Formation of Graphyne on Transition Metal Surfaces: A Competition with Graphene from the Chemical Potential Point of View. *J Phys. Chem. C* 2016, **120**, 14699-14705.

(42) Reuter, K.; Scheffler, M. Composition, Structure, and Stability of RuO_2 (110) as a Function of Oxygen Pressure. *Phys. Rev. B* 2001, **65**, 035406.

(43) Samanta, A.; E, W.; Zhang, S. B. Method for Defect Stability Diagram from Ab Initio Calculations: A Case Study of $SrTiO_3$. *Phys. Rev. B* 2012, **86**, 195107.

(44) Gan, C. K.; Srolovitz, D. J. First-Principles Study of Graphene Edge Properties and Flake Shapes. *Phys. Rev. B* 2010, **81**, 125445.

(45) Curiale, J.; Granada, M.; Troiani, H. E.; Sánchez, R. D.; Leyva, A. G.; Levy, P.; Samwer, K. Magnetic Dead Layer in Ferromagnetic Manganite Nanoparticles. *Appl. Phys. Lett.* 2009, **95**, 043106.

(46) Liu, L.; Ren, X.; Xie, J.; Cheng, B.; Liu, W.; An, T.; Qin, H.; Hu, J. Magnetic Switches via Electric Field in BN Nanoribbons. *Appl. Surf. Sci.* 2019, **480**, 300-307.

(47) Luo, W.; Pennycook, S. J.; Pantelides, S. T. Magnetic "Dead" Layer at a Complex Oxide Interface. *Phys. Rev. Lett.* 2008, **101**, 247204.

(48) Borghi, G.; Fabrizio, M.; Tosatti, E. Surface Dead Layer for Quasiparticles Near a Mott Transition. *Phys. Rev. Lett.* 2009, **102**, 066806.

(49) Han, N.; Yang, D.; Zhang, C.; Zhang, X.; Shao, J.; Cheng, Y.; Huang, W., Role of Buffer Layer and Building Unit in the Monolayer CrI_3 Growth: A First-Principles Perspective. *J Phys. Chem. L* 2020, 11 (21), 9453-9460.